Applying Wind Simulations for Planning and Operation of Real-Time Thermal Ratings

David M. Greenwood, *Member, IEEE*, Grant L. Ingram, and Phil C. Taylor, *Sr. Member, IEEE*

***Abstract*— Real-Time Thermal Ratings (RTTR) is an emerging technology that allows the rating of electrical conductors to be estimated using real-time, local weather observations. In many cases this leads to a very significant (typically 50-100%) increase in rating with respect to conventional approaches. Conductor rating is heavily influenced by wind speed and direction. Consequently in this paper computational wind simulations, commonly employed by the wind energy industry, have been applied to inform rating estimation during network planning and operation. This provides an exciting opportunity to allow the identification of determining conductor spans, to inform network designers of the rating potential of different conductor routes, to estimate the additional wind energy that could be accommodated through the enhanced line rating and to allow intelligent placement of the monitoring equipment required to implement RTTR. The wind simulation data were also used to allow more accurate estimation of conductor ratings during operation. Two case studies taken from actual trial sites in the United Kingdom are presented to demonstrate that these techniques can provide a real world benefit.**

***Index Terms*—Overhead Power Lines, Computational Fluid Dynamics, Power System Planning, Power System Meteorological Factors**

NOMENCLATURE

C	Energy Constraint	[KWh]
$Dx_{i,j}$	Distance between two points, i and j, in the x direction/	[m]
E	Energy	[KWh]
I	Current	[A]
K_s	Roughness Height	[m]
N	The number of observations used in an estimation	
P	Power	[W]
PO	Power Output	
$\bar{r}$	Mean conductor rating	[A]
$S_{i,Wd}$	Speedup characteristic at point I and wind direction Wd	
T	Temperature	[°C]
Wd	Wind direction	
k	Weighting factor between relative speedup factors	
t	time interval to be considered	[h]
u	X Direction Wind Vector	[m.s^{-1}]
$\tilde{u}$	Estimated X Direction Wind Vector	[m.s^{-1}]
v	Y Direction Wind vector	[m.s^{-1}]
V	Voltage	[V]
$\tilde{v}$	Estimated Y Direction Wind Vector	[m.s^{-1}]
$\widetilde{Wd}$	Estimated Wind Direction	[°]
$\widetilde{Ws}$	Estimated Wind Speed	[m.s^{-1}]
z_h	Wind Turbine Hub Height	[m]
z_α	Conductor Height	[m]
θ	Angle of Incidence	[°]
ϕ	Power Factor Angle	[°]

This work was supported by Scottish Power Energy Networks, Airbus Space and Defense and EPSRC.

David M. Greenwood and Phil C. Taylor are with the School of Electrical and Electronic Engineering, Newcastle University, Newcastle Upon-Tyne, UK. (email: david.greenwood@ncl.ac.uk)

Grant L. Ingram is with the School of Engineering and Computing Sciences, Durham University, Durham, UK. (email: g.l.ingram@dur.ac.uk)

I. INTRODUCTION

REAL-TIME Thermal Rating (RTTR) is a technology that allows the current carrying capacity of electrical conductors, which varies with ambient temperature, solar radiation, and wind speed and direction, to be estimated using real-time, local weather measurements [1]. In many cases this leads to an increased rating (typically 50-100%), with respect to conventional approaches, the majority of the time. RTTR, using weather measurements to estimate line ratings and temperatures has been demonstrated internationally in multiple projects [2-4].

A sensitivity analysis by *Michiorri et al.* [5] showed that wind speed has the greatest impact on overhead line (OHL) current carrying capacity by a significant margin. Wind direction also leads to significant variations in current carrying capacity, having a comparable impact to ambient temperature. Wind speed and direction are variable on space scales varying from meters to kilometers, particularly in complex or hilly terrain [6]. Properly accounting for this variation is important for planning and operation of RTTR in power systems.

In the wind energy industry, micro scale numerical wind simulations, based on Computational Fluid Dynamics (CFD), are used to predict energy yields [7], site turbines within a wind farm [8, 9] and evaluate turbine wake effects [10]. In this paper, these methods have been adapted to calculate the wind speeds and directions incident to OHLs, and hence calculate their ratings.

Key challenges in RTTR planning are: predicting potential rating increases before deploying any RTTR hardware to the network; identifying the determining spans, or thermal bottlenecks, within the network; estimating the energy yield of distributed generators connected to networks making use of RTTR and, sensor placement. During operation the key challenge is to estimate conductor current carrying capacity in real time. Solving these problems will provide network

engineers with an array of new tools to enhance their operating and planning capability.

The rest of the paper is structured as follows: Section II introduces the concept of the Atmospheric Boundary Layer; section III discusses the CFD method used to model wind flows; section IV then presents methods for using the CFD results in power network planning, while section V presents a method to use the results for real-time Rating State Estimation (RSE). Real world case studies are provided in each section. In section VI we discuss further research that could improve the estimation in this paper. Finally, conclusions are provided in section VII.

II. The Atmospheric Boundary Layer

The wind flows which affect conductor ratings take place in the Atmospheric Boundary Layer (ABL). This is the layer of air immediately above the Earth's surface, which is directly influenced by the surface through its shape, roughness and temperature [11]. The forces that influence the ABL include frictional drag, evaporation and transpiration, heat transfer, pollutant emission and terrain induced flow modification [12]. This layer is close enough to the Earth's surface that effects that are important in the upper atmosphere can be ignored. The ABL is commonly modelled as neutrally stable, meaning the surface-boundary interaction is a purely mechanical process [13]; this means that frictional drag and terrain induced flow modification, are the parameters which control boundary layer behavior. This assumption is used in this paper.

A. Wind Flow over Terrain

The terrain over which the wind blows can be broken down into two parts; the orography (the ground elevation) and terrain features (what is on the ground). Modelling wind flow over the orography is relatively straight forward; the orography can be used to create a surface geometry around which a CFD mesh can be constructed.

The terrain features can include trees, shrubs, and buildings, which affect wind patterns. Conventionally these features are represented by a so called 'sand grain' roughness on the surface [14]. This roughness modifies the shape of the flow boundary layer depending on the roughness [15], which in turn alters the flow. Since the terrain is modelled as a surface roughness rather than fully realized 3D objects, effects such as sheltering from vegetation are not represented. This means that while the simulations can accurately model changes in the shape of the boundary layer, they do not account for effects such as the wakes behind buildings or woodland [16-18].

B. Flow Solver

Most fluid-flow problems are too complex to be solved analytically. Consequently, they are decomposed into many smaller problems and solved using standard techniques. CFD itself, and wind simulation in particular, are the subject of much ongoing research. However, in this paper we are focused on the application of standard techniques to new power systems applications. For this reason, the CFD calculations were performed using Fluent 12.1, a broadly used, general purpose CFD package. Fluent has been used for wind simulations by other authors, and produced results comparable to dedicated wind modelling software [19, 20].

III. CFD Method

A. Input Data

To construct the CFD model, data is needed to represent the terrain and underlying orography. Orography data was available from the UK Ordinance Survey Digimap service. Grid spacing and starting coordinates were specified and the elevation at each point is provided. These data were used to create a 3D surface model of the orography.

Terrain feature data were provided by Airbus Space and Defense. The data was captured by LiDAR survey [21] and categorized different terrain features by their roughness; these categories were then assigned a roughness height for use in the CFD simulation based on industry standard values [22].

B. Computational Domain

A computational mesh was created around the 3D surface model. The structure and quality of this mesh affect the duration and accuracy of the numerical solutions [23]. For this application, it was important to have a large number of cells close to the terrain, where the most complex interactions take place, and where the power lines were located. The cells then grew in size as they expanded upwards into the ABL. This reduced the computational requirements, but was not detrimental to the results since this was far from the area of interest, and there were few complex interactions at this altitude. An example of a mesh used in this paper is shown in Fig. 1 .

The inlet Boundary Condition (BC) was set as suggested by [24], to represent wind coming into the domain. The terrain was modelled as a rough wall, and the sides and top of the domain were modelled as symmetry (a frictionless wall).

C. CFD Simulations

The aim of the CFD simulations was to create wind data sets that represent the majority of wind conditions experienced at the location of the network. Once a model had been created the data set was generated by altering the prevailing wind direction in 10° steps, resulting in a set of 36 simulations to represent a domain.

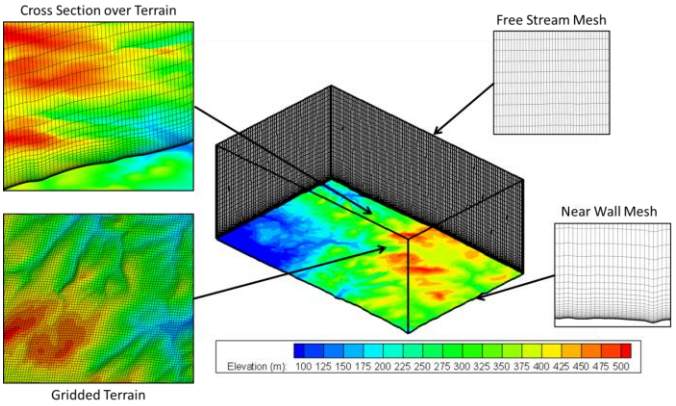

Fig. 1. An illustration of mesh structure, with small cells close to the boundary and larger cells at higher altitudes. The mesh is also refined where the terrain is particularly complex. This illustration shows the structured hexahedral mesh used in this paper.

The results of 3 sets of simulations are discussed in this paper. Bolund Hill, a commonly used test case, was simulated to ensure the methods used were comparable with state of the art wind simulations. The other two sets of simulations were carried out to provide case studies for the paper, both are simulations of wind flow close to Scottish Power Energy Networks' 132kV network in North Wales. One simulation is of the proposed route to a new large wind farm, and was used to demonstrate the planning methods discussed in the paper. The other model encompasses existing 132kV network, and was used to validate the online state estimation. Details of the meshes created and simulations performed are provided in Table I.

Table I: Details of the CFD meshes created for the study and the number of simulations run

Mesh Name	*Number of Cells*	*Number of Simulations*
Bolund Hill	3.5 Million	4
Planning Case Study	3.5 Million	36
State Estimation Case Study	2.8 Million	36

D. CFD Validation using Bolund Hill

A validation exercise was conducted using the Bolund Hill experiment [25]. Bolund hill is a 12m high costal hill situated in Denmark [26]. In 2007/2008 ten wind masts were set up, with a total of 35 monitoring stations on and around the hill for a period of three months to record the effect of the hill's complex topography on local wind flow. This data has since been used to validate computational wind simulation packages and CFD simulations [27] including Windsim [28], WASP and general purpose RANS based packages.

Simulations were performed modelling the hill using the method described in sections B and C. The resulting average error of 7.5% was comparable to the best simulations submitted to the Bolund Experiment [27], whose average errors varied from 4% to 10%.

IV. Network Planning with CFD Wind Modelling

A. Creating Data Representative of Local Wind Regimes

The CFD results are used to generate a grid of normalized wind speeds, known as speedup values. This is done by taking a surface of points at a set height above the ground, and dividing the velocity magnitude at each point by the mean velocity magnitude across the domain, as shown in equation (1). All of the examples presented here take the surface at 10m above ground level. This is because 10m is the height at which wind speed measurements are generally taken [29], and 10m provides a reasonable approximation to the height of overhead conductors.

$$S_i = \frac{\widehat{Ws}_i}{\frac{\sum_{j=1}^{n} \widehat{Ws}_j}{n}} \qquad (1)$$

In equation (1), the value S_i is the Speedup value at point *i*, $\widehat{Ws}$ is the simulated wind speed and *n* is the number of points. A database of these Speedup values must be computed for each set of inlet conditions input to the CFD model.

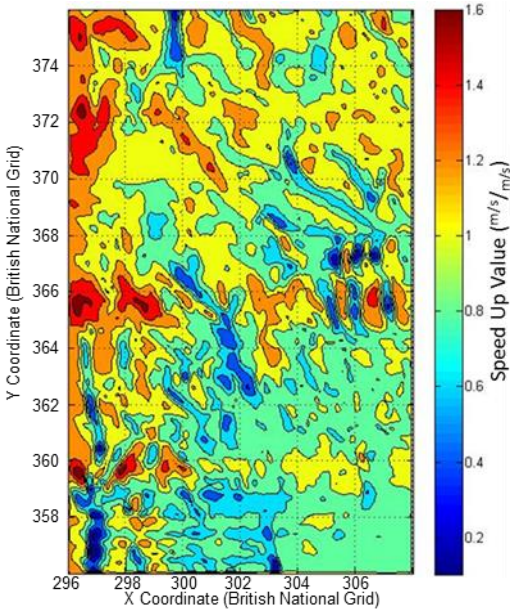

Fig. 2. Example of a contour plot of speed up characteristics

Fig. 2 shows a contour plot of Speedup values at 90° inlet condition (an easterly wind), from the planning case study. It illustrates the high level of spatial variation. If a conductor was running from the north to the south of the domain, with a weather station roughly every 10km (the spacing used in Scottish Power's demonstration project [30]), it would pass through areas where the wind speed varies from 20% to 120% of the average value, which would not be accounted for by observations.

For the studies described, local wind speed, direction and temperature data were provided by the UK Met Office. These Local measured data were combined with the Speedup data to create an hourly data set. For each time step in the hourly data set, the appropriate Speedup data should be selected based on the measured wind direction, *Wd*. This is then multiplied by the measured wind speed, *Ws*, to give time series of estimated wind speed, $\widehat{Ws}$, for every point in the domain, as shown in equation (2):

$$\widehat{Ws}_i = S_{i,Wd} \cdot Ws \qquad (2)$$

These time series were used to evaluate the benefits that could be provided through RTTR, identify where thermal bottlenecks are likely to be located and assist in the optimal placement of monitoring equipment. The methods devised to calculate these are described in sections B-F.

B. Average Rating Calculation

Though knowing the average rating of a conductor does not give a complete understanding of its behavior, it is a useful tool for knowing where critical spans are likely to occur. The average rating can be obtained by calculating the rating at each time step, or by calculating average weather conditions and using these to estimate the average rating.

The ambient temperature values from the historical weather data can be applied directly, since temperature has a relatively low variation over the space scales of an OHL. If several sets of temperature data were available, then inverse distance

interpolation can be used to calculate the appropriate value [2].

Wind direction should be assumed to be 0° relative to the conductor at this stage (a worst case assumption), and solar radiation should be ignored.

C. Critical Span Identification

In many cases, the rating of a circuit can only be as high as the rating of its lowest rated section. Consequently it is important to identify which span, or spans, this is likely to be. It may be necessary to add extra instrumentation here, or even to re-conductor just one span. Average annual rating values provide a good initial estimate of where a critical span is likely to be located. The location of the network can be superimposed over the estimated ratings, and spans that cross areas with low average ratings can be identified.

The wind direction relative to the line was assumed to be 0° (the worst case scenario) for the average rating calculations. However, the prevailing wind direction at each point in the CFD domain can be calculated in the same way as the average wind speed. This can be combined with the angle correction factor shown in Fig. 3 to calculate the average annual rating of a conductor. Equation (3) shows how to calculate this corrected mean rating, $\bar{r}_{corrected}$, from the mean rating $\bar{r}$, the correction factor *CF*, and the difference between the orientation of the conductor θ_c and the mean wind direction *Wd*.

$$\bar{r}_{corrected} = \bar{r}.CF(\theta_C - Wd) \qquad (3)$$

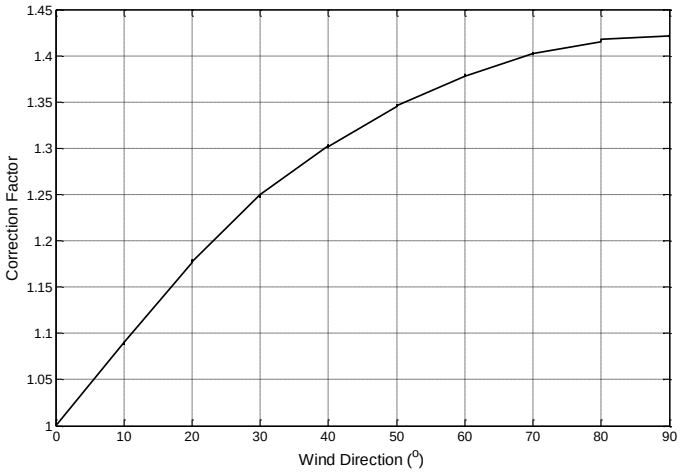

Fig. 3. Wind direction correction factors for conductor rating, calculated based on a sensitivity analysis undertaken by the authors.

These average rating values can be used to identify where critical spans are likely to occur, or to identify areas that are likely to maximize benefits or minimize the risks from RTTR.

D. New Conductor Siting

The siting of new OHLs is a complex process. Various steps must be taken including environmental surveys and planning consultations [31]. The conductor is often sited where it will have the least visual impact, such as in a valley or behind a tree line; this is directly at odds with obtaining the greatest benefit from RTTR. If RTTR was considered at the planning and design stage, it would be possible to factor the potential benefits into the planning process. This could lead to situations where fewer circuits need to be built, or lower rated conductors can be used. One example is that rather than building a steel tower line through a valley, a wood pole could be built along a ridge.

The method for siting new OHLs is similar to the method

$$I_{WF} = \frac{P}{3Vcos\emptyset} \qquad (4)$$

for identifying critical spans. Rather than looking at the average rating at the location of the existing conductors, the average rating at the location of proposed route corridors can be examined. In some cases, it may even be possible to plan conductor routes perpendicular to prevailing wind flows.

E. Wind Farm Energy and Constraint Assessment

While the average rating is a reasonable indicator of which conductors are likely to be critical spans, it does not give an indication of when the additional capacity is available. This is relevant if the circuit is being used to connect wind generation, because it is important to know how high the rating of the conductor will be when the wind farm is working at rated capacity. Lines with a low average rating could be sufficient to facilitate additional wind generation if their periods of high rating coincide with high wind speed, and hence high generation, at the wind farm site.

The CFD model can be used to give an indication of where high wind speeds occur in the area of interest concurrently with high wind speeds at the wind farm site. The following steps are taken:

- Select a point in the domain to represent the wind farm location. This makes the assumption that the wind farm, which covers a large area, can be adequately represented by one point.
- Calculate time series of wind data for the time interval to be considered, *t*, at the location of the wind farm and the possible locations of the conductors.
- Wind turbine hub height is often around 100m, so the 10m wind speed must be scaled up to give the speed at turbine hub height, using standard wind height correction in equation (5) [2]:

$$\widetilde{Ws} = \widetilde{Ws}_{\alpha} \cdot \left(\frac{z_h}{z_{\alpha}}\right)^{kshear} \qquad (5)$$

$\widetilde{Ws}$ is the simulated wind speed at the height of the turbine hub, $\widetilde{Ws}_{\alpha}$ is the simulated wind speed at conductor height, z_h is the turbine hub height and z_{α} is conductor height (assumed to be 10m). *Kshear* is a ground roughness value. Appropriate values of *Kshear* for different ground types can be found in [32]. Alternatively, the speed up value could be taken from the simulation at turbine hub height. However, this method allows several turbines with varying hub heights to be compared, without having to extract additional data from the CFD results

- Use the wind speed at this location to calculate the wind farm power output.
- Use the wind data at the conductor sites, along with temperature data if available, to calculate the conductor rating at the sites of the conductors.
- Scale the wind power output by the maximum output of the wind farm:

$$P = P_{Rated}.PO \quad (6)$$

- Calculate the current in the line:

Where I_{WF} is the line current produced by the wind farm and $\emptyset$ is the power factor angle. Assuming unity power factor:

$$I_{WF} = \frac{P}{3V} \quad (7)$$

- At each point in the time series, compare the power to the line rating and evaluate the constraint and energy yield:

$$C = 3V \cdot \sum_{t=0}^{T} \begin{cases} I_{WF} - r > 0, I_{WF} - r \\ I_{WF} - r < 0, 0 \end{cases} \quad (8)$$

$$E = \sum_{t=0}^{T} P_t - C \quad (9)$$

$$C_{prop} = \frac{C}{\sum_{t=0}^{T} P} \quad (10)$$

In equations (8)-(10) r represents the conductor rating in amps, C represents energy that must be curtailed from the windfarm due to network constraints, E represents the total energy yield after constraints and C_{prop} is the constraint as a proportion of the available energy yield.

This method can be used to consider wind farms with a variety of energy capacities, ranging from those that would be permitted by the static ratings, to those with peak power outputs greater than the conductors would conventionally allow. This could allow network planners and designers to offer connection agreements to windfarms with greater capacity based on predicted levels of constraint.

F. Where to Instrument

In any RTTR deployment it is essential to have adequate instrumentation to be able to infer the ratings throughout the system. However, the instrumentation can be expensive, particularly in the case of purpose-built devices. Consequently it is prudent to plan a deployment that minimizes the cost of instrumentation without compromising observability. The authors suggest that meteorological observation stations should be sited in locations that are representative of large areas. Other instrumentation, such as sag/tension monitors should be deployed in areas that are not well represented by the weather stations or are likely to contain determining spans.

To determine which areas are appropriate sites for meteorological stations, and which parts of the network will require additional instrumentation, the correlation structure of the domain must be determined. The example shown below uses wind speed correlations, since this is the parameter that varies the most on the relevant space scales. However, it would be equally valid to use the correlation between predicted rating values. The correlation structure was calculated as follows:

- Create time series of wind speed at each point in the domain using CFD results and historical data.
- Calculate the correlation between each pair of time series using equation (11).

$$corr(X,Y) = \frac{cov(X,Y)}{\sigma_x \sigma_y} = \frac{E[(X-\mu_x)(Y-\mu_y)]}{\sigma_x \sigma_y} \quad (11)$$

- Large domains may need the data reducing to make this computationally manageable.
- Equation (11) represents the product-moment correlation between two variables, X and Y, defined by the covariance divided by the product of the standard deviations [33].
- This will yield a matrix of correlations, where element i,j represents the correlation between locations i and j. Taking the mean of each column will give the average correlation between that element and the rest of the domain.
- These average correlations can then be plotted against their positions, showing which areas are well correlated, and which are comparatively independent. An example is shown in Fig. 4

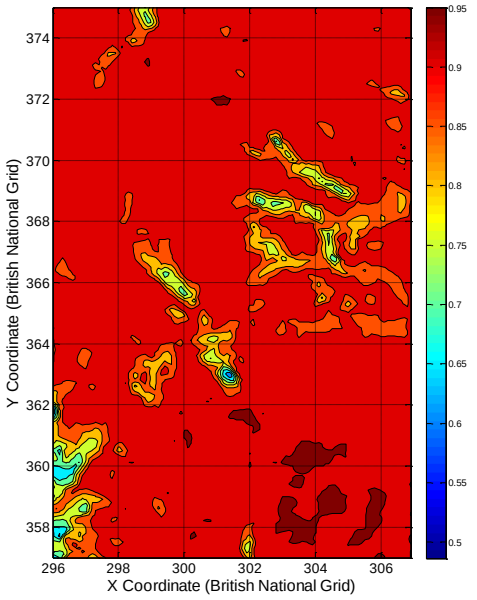

Fig. 4. Average point correlation with the other points in the domain.

The red areas in Fig. 4 show locations that have a high correlation with the rest of the domain. Meteorological stations in the red areas would be able to give a strong representation of the majority of other locations. The yellow and blue areas represent sites with a lower correlation to the rest of the domain. These areas have wind conditions that are not generally representative of the domain; if conductors pass through these areas, additional instrumentation should be deployed to ensure that the system observability is high. This is especially true if these areas have been identified as containing critical spans.

In the majority of cases, the number of locations where sensors, particularly meteorological stations, can be placed may be limited; for example they may only be placed at substations, where they are guaranteed power and data connections. However the method presented is still valid for suggesting which of these locations would provide the best coverage, and which could provide redundant cover of well monitored areas. Limited options would also reduce the computational burden of calculating the correlation structure.

G. Case Study

1) Description of Case Study

The case study was located in north Wales, just south of the city of St Asaph. Several new onshore wind farms were attempting to connect to the 132kV network, which required the construction of a new OHL. The potential routes for this line are shown in Fig. 5, along with the location of the existing network and the wind farm site. The proposed OHL had a static summer rating of 89MVA. This study aims to quantify whether additional wind generation could be connected using RTTR [34]. The case study therefore is a realistic industry test case and not a highly abstract lab based study.

2) Studies Undertaken

A CFD mesh of the trial site, shown in Fig. 1, was created. 36 simulations were performed, altering the inlet condition by 10° for each simulation, to give representations of the wind regime for a variety of prevailing wind conditions. The goals of the case study were to identify which OHL route would result in the greatest energy yield from the wind farm, to calculate the size of wind farm that could be accommodated and to estimate the energy yield and constraints for the wind farm.

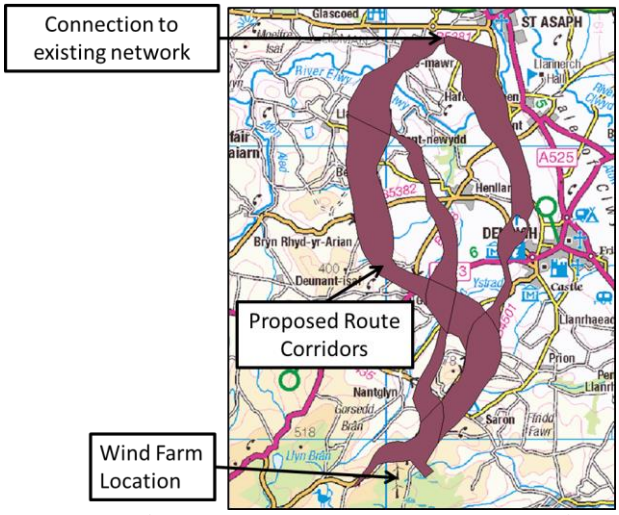

Fig. 5. A map of the case study area showing the route corridors for potential OHLs and the elevations of the local terrain.

The method described in section IV B was applied to calculate the average ratings throughout the domain, as shown in Fig 6. The ratings are shown as a proportion of the seasonal ratings [35] to give an indication of the additional capacity available. These ratings suggest that the central route corridor would allow the wind farm with the greatest generating capacity to be connected. However, while this route had the greatest mean capacity, it did not necessarily have high ratings concurrently with high generation at the wind farm. The method described in section IV E was applied to evaluate energy throughput, considering wind farms with an 80, 100, 120 and 140MW capacity.

A consequence of connecting a wind farm with a greater capacity than the rating suggests the circuit can support is that the generator will sometimes have to be constrained. There have been a number of studies on constrained wind farm connections demonstrating that this is a realizable solution [36, 37]. Fig. 7 shows time series of conductor rating and the current arising from the wind farm. It can be seen that the two follow the same trends, and that the wind farm occasionally exceeds the conductor rating, which would lead to a constraint. Table II shows the constraint in energy yield for the wind farms considered in this study. There is a clear business case for a windfarm with a 140MW rating with a predicted constraint of 1.1% of energy yield.

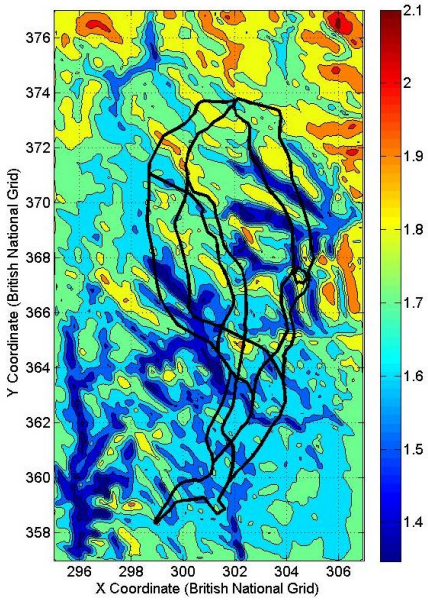

Fig. 6. Map of annual average conductor rating as a proportion of seasonal ratings. The locations of the approved route corridors are shown on the plot.

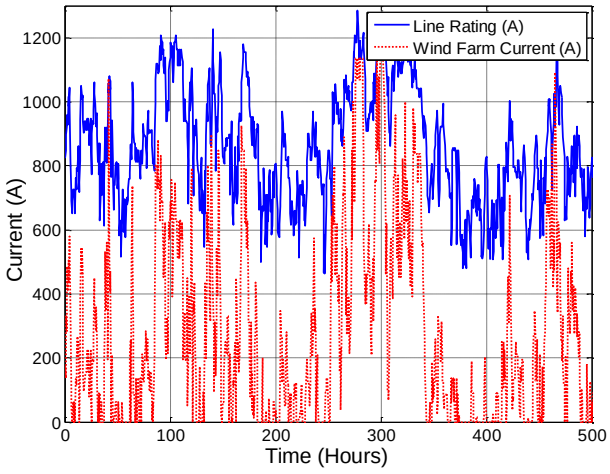

Fig. 7. Time series of conductor rating and wind farm current from a 120MW Wind Farm.

Table II: Energy yield constraints for wind generators of different capacities

Wind Farm Capacity (MW)	*Constraint (% of energy yield)*
80	0.01
100	0.35
120	0.7
140	1.1

V. Real-Time Rating State Estimation

A. Motivation

Weather based RTTR offers wide coverage of network current carrying capacity while using relatively few instruments [2] compared with line monitoring devices. However, the existing techniques for applying weather based RTTR use simple interpolation methods to estimate the weather conditions, and hence the rating, throughout the system. This method does not account for the variability of wind on the relevant space scales [6, 38], resulting in errors in RSE. Given that wind speed and direction have a significant impact on conductor current carrying capacity, wind simulations can provide detailed information about how the terrain affects the local wind flow. However, the simulations are time consuming and consequently cannot be run during operation. This is because the thermal time constant of an overhead conductor requires the rating to be updated every 10 minutes to avoid exceeding the conductor's design temperature [39]. Consequently, a method was required to allow detailed simulation results to be applied in an operational timeframe. The proposed method uses a database of CFD results – which have been calculated offline – to allow RSE to be carried out quickly enough to calculate the rating within the conductor's thermal time constant.

B. Method

The CFD simulations provide a relationship between the terrain and the wind flow. The next step is to use this relationship to estimate conductor ratings. The RSE takes place at discrete time intervals, with the calculated rating being applied for the next time step – these time steps should be no longer than 10 minutes [39]. This method assumes that a weather based RTTR system is being deployed, with several meteorological stations sited throughout an area of network.

Each time step, the most representative set of wind simulation data must be selected from the database. This is done by normalizing the observed wind speeds by the mean observed wind speed, comparing them to each set of simulation results and minimizing the error in *X* and *Y* direction vectors.

$$\widehat{Ws}_N = \frac{\widehat{Ws}}{\frac{\sum_{j=1}^{m} \widehat{Ws}_j}{m}} \tag{12}$$

$$S_{BF} = arg\min_{i=1,n} \sum_{j=1}^{m} \left[(u_{Nj} - Sx_{i,j})^2 + (v_{Nj} - Sy_{i,j})^2 \right] \tag{13}$$

$$\tilde{v}_i = Sy_j \left(\sum \frac{\sum_{j=1}^{m} Ws_j}{m} \right) \tag{14}$$

The measured and calculated values were decomposed into *x* and *y* direction vectors. In this paper, *z* direction flows were not considered because the available weather data did not contain *z* direction values. This is a conservative assumption, since if the *z* direction values were included the overall wind velocity and hence cooling effect, would be increased.

The ambient temperature and incident solar radiation were estimated using inverse distance squared interpolation as in the RTTR methodology described by *Michiorri et al* [2].

C. Case Study

The case study presented in this paper is the same as that used by *Michiorri et al.* [2]. It was a section of 132kV distribution network located in north Wales. The area of interest spanned 20km, with five meteorological stations deployed across the network. A map of the local area depicting the location of the meteorological stations and overhead conductors is shown in Fig. 8. The meteorological stations provided the average temperature, wind speed, wind direction and solar irradiance every 5 minutes.

The area included towns, wooded areas, hills and valleys. The elevation varied from sea level to 304m. OHLs ran parallel to the north coast of Wales, approximately 6km inland. The conductors used in the study were generally under-utilized; however, proposed onshore and offshore wind farm developments meant that in the next few years the circuits were expected to be at capacity, making it an ideal test area for RTTR. This again is representative of industrial practice and provides a credible example of how these techniques will be deployed in real engineering systems.

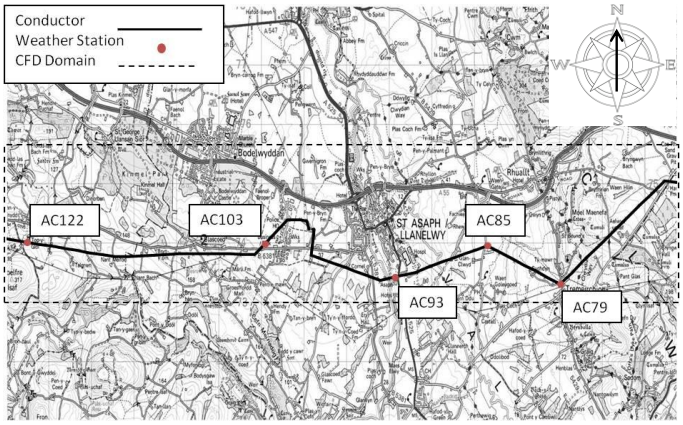

Fig. 8. A map of the trial site area, showing local features and the location of the meteorological stations and conductors

1) CFD Results

To validate the wind speed estimation, the CFD model was used to estimate the wind speed at each meteorological station using the data from the other four stations as an input. This was calculated using a year of observed data, and the results are shown in Table III.

Table III: Mean absolute errors in wind speed and direction estimation using the CFD Method

	AC93	***AC85***	***AC79***	***AC103***	***AC122***
Average CFD Error (m/s)	2.01	1.00	0.98	1.04	2.62
Average CFD Error (°)	48.1	35.1	43.5	50.6	42.1

The errors in wind speed and direction estimation are shown in Table III. In three cases, the MAE (mean absolute error) in wind speed estimation was around 1m/s. At weather stations AC93 and AC122 the MAE was much higher. AC93 is directly to the south of the city of St Asaph. The city is represented in the simulations by a sand grain roughness model; while this alters the shape of the boundary layer appropriately, it will not create the wake effect that would be caused by the town in reality. If station AC93 is in this wake, that could account for the high estimation errors. AC122 was

far from the other measurement stations so, given that the other observations are used as an input to the estimation, it is not surprising that the highest error was recorded here. These are examples of areas where line monitoring may be more appropriate than a purely weather based approach.

2) Real-Time Thermal Rating Results

The aim of this work was to determine whether the CFD wind simulation results could be used in online state estimation. A validation was performed by estimating the rating at each meteorological station using observations from the other 4. Fig. 9 shows the calculated rating using the new CFD method, compared with the actual ratings. The estimated rating follows the trends in the measured rating, but often misses high frequency changes.

Table IV shows the MAE in rating estimation using the CFD method, compared with the previously implemented inverse distance interpolation method [33]. There are larger errors at AC122, the most remote weather station, and AC93, corresponding to the high wind speed and direction errors. Wind simulations are used by the wind industry to assess long term aggregates in energy yield, so it is not surprising that a real-time application, trying to capture short term variations, results in higher errors. Improvements in both wind simulation and state estimation could reduce this error, but it is encouraging that reasonable results can be obtained using the simple methods presented in this paper.

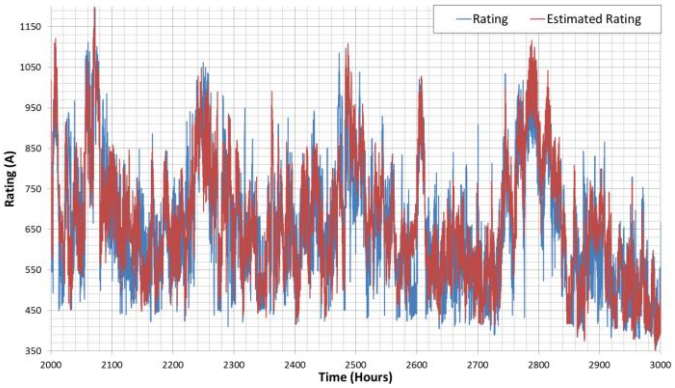

Fig. 9. Comparison of CFD rating estimation and measured values

Table IV: A Comparison of mean absolute error in rating prediction between the inverse distance and CFD methods

	AC93	*AC85*	*AC79*	*AC103*	*AC122*
CFD Rating Error (A)	161.5	93.9	86.4	102.7	176.2
CFD Rating Error (%)	28.3	13.6	12.5	14.2	21.1
Interpolation Ratings Error (A)	145.5	118.6	97.7	88.3	180.6
Interpolation Ratings Error (%)	25.5	17.2	14.1	12.21	21.6

D. Alternative Interpolation Method

Although the method discussed in section V.B gave good agreement between the measured and estimated wind speeds at 3 of the stations (mean absolute errors of around 1 m/s), the error at the other two stations – and particularly the most remote station, AC122 – were too high for realistic implementation. Consequently, a new state estimation method, hybridizing the method from section V.B and the original linear interpolation method has been developed and is described here.

Rather than using the global average wind speed, the X and Y wind speed vectors are used, in conjunction with a relative speedup value, which is calculated thus:

$$Sx_{i,j} = \frac{Sx_i}{Sx_j} \tag{15}$$

So for any estimation, there will be N speedup values for each direction, which must then be combined through some weighting mechanism to give an estimate for the wind velocity.

$$\tilde{u}_i = \frac{\sum_1^N \frac{u_j . S_{i,j}}{Dx_{i,j}^k}}{\sum_1^N \frac{1}{Dx_{i,j}^k}}, \tilde{v}_i = \frac{\sum_1^N \frac{v_j . S_{i,j}}{Dy_{i,j}^k}}{\sum_1^N \frac{1}{Dy_{i,j}^k}} \tag{16}$$

Where $Dx_{i,j}$ is the distance between the point i and the station j in the x direction and k is a constant, obtained through an optimization based on minimizing estimation error at the points where the wind velocity is known (i.e. the weather station sites).

E. Results

The results using the alternative interpolation method are shown in Table V. Overall, the error in both speed and direction estimation has been reduced compared to the original method. However, the improvement is not uniform and, particularly in the case of AC85 and AC79where the speed estimation error is actually slightly worse. This is counteracted by the improvement in direction error, which results in a reduction in rating estimation error at every station bar AC85.

Table V: A Comparison of mean absolute error in rating prediction between the inverse distance and the Alternative Interpolation

	AC93	*AC85*	*AC79*	*AC103*	*AC122*
Mean Angle Error (°)	38.33	27.84	34.66	38.69	36.88
Mean Speed Error (m/s)	1.40	1.22	1.05	1.00	2.28
CFD Rating Error (A)	129.68	103.67	84.75	93.40	149.88
CFD Rating Error (%)	18.76	15.02	14.85	12.91	17.95

These results represent the first of several possible further work streams to improve the state estimation, and to bring the exciting possibilities offered by CFD to real network operation.

VI. Future Research to Improve Estimation

Although the methods used in this paper have demonstrated the potential for wind simulations to inform RTTR, the authors recognize that this research is a first step. This section contains suggested improvements to the methods discussed in this paper which could be the subject of future research.

A. Improved CFD Methods

Further work could seek to improve the CFD set up for wind flow estimation. The BC in the existing solution assumes a uniform wind flow across the inlet to the domain. In reality, it is unlikely that this is the case. Instead, it could be

preferable to construct non-uniform BCs, based on the observed wind speeds and directions within the domain, with some interpolation applied between them. The difference between the two BCs is shown in Fig. 10.

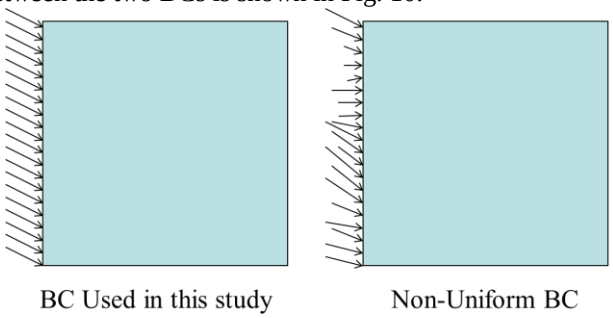

Fig. 10. The difference between a uniform and non-uniform inlet BC

Alternatively, the inlet condition could be determined by running a simulation on a much larger domain and using the results from this at the location of the inlet to the original domain to determine the new inlet condition.

In the existing CFD set up, the surface roughness data is represented in the simulation as roughness elements at ground level. The function of these elements is to distort the shape of the boundary layer in the same way as the physical object the roughness element represents. However, since the roughness elements are at the same height as the ground, the roughness elements do not provide the same wake effect as the physical objects. This is apparent in the simulations, where AC93 is situated next to an urban area, and as a result the CFD over estimates the wind speeds at that location. Using fully realized objects, rather than a simple surface roughness model, could account for these wake effects, albeit at the cost of more computational time and resources. This method could account for the effect of trees and other vegetation near to the line much more accurately than the existing method. The difference between the two roughness models is shown in Fig. 11.

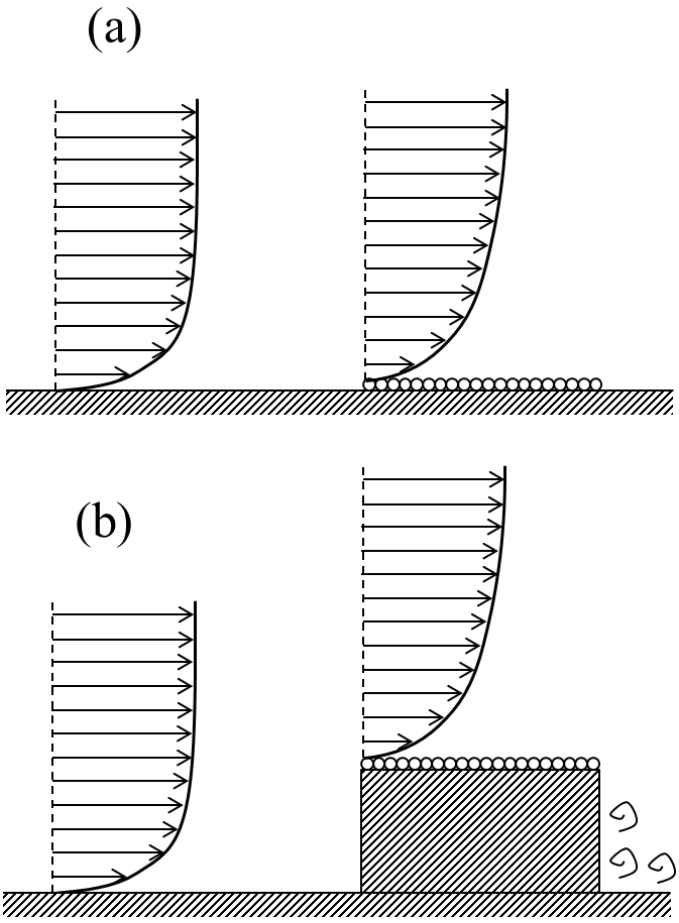

Fig. 11. (a) shows the effect of roughness elements on a boundary layer, while (b) illustrates that in reality the boundary layer is also shifted physically upwards, and a wake is created behind the roughness object. This could be woodland, vegetation or a building.

B. Size of CFD Results Databases

The research carried out so far relies on a database of 36 CFD simulations, created by varying the inlet condition by 10^o for each simulation. The accuracy of the method could be improved by expanding the size of this database, both through increasing the resolution (for example simulations every 5^o) and through creating more representative inlet boundary conditions as suggested in section VI. A.

VII. CONCLUSIONS

This paper has demonstrated how wind simulations can be used to provide information about wind flows local to RTTR schemes, both in network planning and operation. Planning methods were proposed, using concepts commonly applied in the wind energy industry, to identify thermal bottlenecks in the network, allow RTTR informed planning of new network assets, inform sensor placement and allow network operators to see the potential benefits of RTTR prior to deployment. A time series analysis method was described to calculate the constraints and energy yield of new wind farms.

A case study using a real wind farm connection was presented. The results suggested that it would be possible to connect a wind farm with a generating capacity of 140MW to a circuit with a static rating of 89MVA with generating constraints of only 1.1%. The results also show that the route of the OHL could make a significant difference to the energy yield from the wind farm.

Most importantly, these methods can allow network planners and designers to estimate how much additional capacity will be provided through RTTR before deploying any equipment to the network. Furthermore, the methods can be used in the planning of new assets, allowing these to be appropriately selected and located to maximize the benefit of RTTR.

A method for estimating wind speeds and directions in a weather based RTTR system was also developed. Existing interpolation based methods [2] took no account of the relationship between terrain orography and wind flows. This new method allows that relationship between terrain and conductor rating to be accounted for. By coupling pre-calculated wind speed and direction values with real time observations, the method allows conductor ratings to be calculated quickly, which is essential to avoid conductors exceeding their design temperature. The method provided

reasonable estimation, though the errors were higher than is desirable for operation, particularly in certain circumstances. Means of potentially improving the estimation were proposed as the subject of further research.

This paper therefore describes a rich set of new tools for network planners and operators that have been demonstrated on two real world case studies. The authors expect in future that real time thermal rating deployments will become as ubiquitous as static ratings are today on the network and that these techniques will also be routinely used in network planning and operation.

REFERENCES

[1] D.M. Greenwood, J.P. Gentle, K.S. Myers, P.J. Davison, I. J. West, G.L. Ingram, *et al.*, "A Comparison of Real Time Thermal Rating Systems in the U.S. and the UK," *IEEE Trans. Power Delivery*, vol. 29, pp. 1849-1858, 2014.

[2] A. Michiorri, P. C. Taylor, and S. C. E. Jupe, "Overhead line real-time rating estimation algorithm: description and validation," *Proc. IMechE Part A: J. Power and Energy*, vol. 224, pp. 293-304, 2010.

[3] A. Michiorri, Currie, R., Taylor, P., Watson, F., Macleman, D. , "Dynamic line rating deployment on the orkney smartgrid," presented at the 21st Int. Conf. on Electricity Distribution, Frankfurt, 2011.

[4] J. P. Gentle, K. S. Myers, J. W. Bush, S. A. Carnohan, and M. R. West, "Dynamic Line Rating systems: Research and policy evaluation," in *PES General Meeting | Conference & Exposition, 2014 IEEE*, 2014, pp. 1-5.

[5] A. Michiorri, P. C. Taylor, S. C. E. Jupe, and C. J. Berry, "Investigation into the influence of environmental conditions on power system ratings," *Proc. IMechE Part A: J. Power and Energy*,Vol. 223, pp. 743-757, 2009.

[6] A. Agüera-Pérez, J. C. Palomares-Salas, J. J. González de la Rosaa, and A. Moreno-Muñoza, "Spatial persistence in wind analysis," *Journal of Wind Engineering and Industrial Aerodynamics*, vol. 119, pp. 48-52, 2013.

[7] P. Torres, J. van Wingerden, and M. Verhaegen, "Modeling of the flow in wind farms for total power optimization," in *9th IEEE International Conference on Control and Automation* 2011, pp. 963-968.

[8] S. Al-Yahyai, Y. Charabi, and A. Gastli, "Optimal micro-siting of small wind turbine using numerical simulation," in *7th IEEE GCC Conference and Exhibition* 2013, pp. 28-32.

[9] J. M. L. M. Palma, F. A. Castro, L. F. Ribeiro, A. H. Rodrigues, and A. P. Pinto, "Linear and nonlinear models in wind resource assessment and wind turbine micro-siting in complex terrain," *Journal of Wind Engineering and Industrial Aerodynamics*, vol. 96, pp. 2308-2326, 2008.

[10] A. Makridis and J. Chick, "Validation of a CFD model of wind turbine wakes with terrain effects," *Journal of Wind Engineering and Industrial Aerodynamics*, vol. 123, Part A, pp. 12-29.

[11] J. R. Garratt, *The Atmospheric Boundary Layer*: Cambridge University Press, 1992.

[12] R. B. Stull, *An Introduction to Boundary Layer Meteorology*: Springer Netherlands, 1988.

[13] D. M. Hargreaves and N. G. Wright, "On the use of the kâ€“ model in commercial CFD software to model the neutral atmospheric boundary layer," *Journal of Wind Engineering and Industrial Aerodynamics*, vol. 95, pp. 355-369, 2007.

[14] D. G. Blumberg and R. Greeley, "Field studies of aerodynamic roughness length," *Journal of Arid Environments*, vol. 25 (7), pp. 39-48, 1993.

[15] H. Schlichting, K. Gertsen, *Boundary Layer Theory*: Springer, 2000.

[16] A. M. Endalew, M. Hertog, M. A. Delele, K. Baetens, T. Persoons, M. Baelmans, *et al.*, "CFD modelling and wind tunnel validation of airflow through plant canopies using 3D canopy architecture," *International Journal of Heat and Fluid Flow*, vol. 30, pp. 356-368, 4// 2009.

[17] J. C. Lopes da Costa, F. A. Castro, J. M. L. M. Palma, and P. Stuart, "Computer simulation of atmospheric flows over real forests for wind energy resource evaluation," *Journal of Wind Engineering and Industrial Aerodynamics*, vol. 94, pp. 603-620, 8// 2006.

[18] D. Hertwig, G. C. Efthimiou, J. G. Bartzis, and B. Leitl, "CFD-RANS model validation of turbulent flow in a semi-idealized urban canopy," *Journal of Wind Engineering and Industrial Aerodynamics*, vol. 111 (12), pp. 61-72, 2012.

[19] D. Cabezon, Iniesta, A., Ferrerm E., Marti, I., "Comparing WASP and FLUENT for highly complex terrain and wind prediction," Wind Energy, Springer, 2007.

[20] W. Pattanapol, Wakes, S.J., Hilton, M.J., Dickinson, K. J. M. , "Modeling of Surface Roughness for Flow over a Complex Vegetated Surface," *World Academy of Science, Engineering and Technology*, vol. 32, pp. 273-281, 2007.

[21] Astrium Geo-Information Services. (2014, 04/02/2014). *LiDAR Acquisition*. Available: http://www.astrium-geo.com/sg/3254-lidar

[22] W. F. Chen, *Handbook of structural engineering*: CRC Press, 1997.

[23] R. Peyret, *Handbook of computational fluid mechanics*: Academic Pr, 1996.

[24] P. J. Richards and S. E. Norris, "Appropriate boundary conditions for computational wind engineering models revisited," *Journal of Wind Engineering and Industrial Aerodynamics*, vol. 99, pp. 257-266, 2011.

[25] J. B. A. Bechmann, M.S. Courtney,H.E. Jørgensen, J.Mann and N.N.Sørensen., "The Bolund Experiment: Overview and Background.," Risø DTU, National Laboratory for Sustainable Energy Roskilde, Denmark2009.

[26] J. Berg, J. Mann, A. Bechmann, M. Courtney, and H. Jørgensen, "The Bolund Experiment, Part I: Flow Over a Steep, Three-Dimensional Hill," *Boundary-Layer Meteorology*, vol. 141, pp. 219-243, 2011.

[27] A. Bechmann, N. Sørensen, J. Berg, J. Mann, and P. E. Réthoré, "The Bolund Experiment, Part II: Blind Comparison of Microscale Flow Models," *Boundary-Layer Meteorology*, vol. 141, pp. 245-271, 2011.

[28] D. E. Weir, Meissner, C., Gravdahl, A. R., "CFD Validation: A Simple Approach," in *EWEA Event 2011*, Brussels, 2011.

[29] "MIDAS land surface station data," U. M. office, Ed., ed, 2006.

[30] G. Murphy, "Implementation of Real-Time Thermal Ratings," Scottish Power Energy Networks2013.

[31] F. Kiessling, P. Nefzger, U. Kaintzyk, and J. F. Nolasco, *Overhead Power Lines: Planning, Design, Construction*: Springer, 2003.

[32] IEC, "IEC 60826, "Loading and strength of overhead transmission lines"," ed, 1991.

[33] F. E. Croxton, D. J. Cowden, and S. Klein, *Applied General Statistics*: Pritman, 1968.

[34] D M Greenwood, G L Ingram, P C Taylor, S C Brown, and A. Collinson, "Network Planning Case Study Utilising Real-Time Thermal Ratings and Computational Fluid Dynamics," in 22nd Int. Conf. on Electricity Distribution, Stockholm, 2013.

[35] "Engineering Reccomendation P27: Current Rating Guide for High Voltage Overhead Lines Operating in the UK Distribution System," ed. London: Energy Networks Association, 1986.

[36] R. A. F. Currie, G. W. Ault, R. W. Fordyce, D. F. MacLeman, M. Smith, and J. R. McDonald, "Actively Managing Wind Farm Power Output," *IEEE Trans. Power Syst,*, vol. 23, pp. 1523-1524, 2008.

[37] S.C.E. Jupe, P.C. Taylor, and A. Michiorri, "Coordinated output control of multiple distributed generation schemes," *Renewable Power Generation, IET*, vol. 4, pp. 283-297, 2010.

[38] H. M. N. P. Schell, J.L. Lilien, "Quantifying the limits of weather based dynamic line rating methods," in *CIGRE Canada Conference on Power Systems*, Hlifax, Canada, 2011.

[39] J. Hosek, P. Musilek, E. Lozowski, and P. Pytlak, "Effect of time resolution of meteorological inputs on dynamic thermal rating calculations," *Generation, Transmission & Distribution, IET*, vol. 5, pp. 941-947, 2011.

David M. Greenwood (M'14) received an MEng degree in new and renewable energy from Durham University, Durham UK in 2010 and a PhD, for work on real-rime thermal ratings, from Newcastle University, Newcastle upon Tyne, UK, in 2014.

He currently works as a Research Associate at Newcastle University, Newcastle, UK, on projects focusing on energy storage and smart micro grids in developing nations.

Grant L. Ingram receive an MEng from Durham University, Durham, UK in 1997, and a PhD from the same institution in 2003.

He is currently a senior lecturer at Durham University, Durham, UK, and his research focusses on turbo machinery and renewables, approaching both from a fluid dynamics background.

Dr Ingram is a chartered engineer.

Philip C. Taylor (SM'12) received an Engineering Doctorate in the field of intelligent demand side management techniques from the University of Manchester Institute of Science and Technology (UMIST), Manchester, UK in 2001.

He is currently Director of the Newcastle Institute for Research on Sustainability and holds the Chair of Electrical Power Systems in the School of Electrical & Electronic Engineering at Newcastle University, Newcastle upon Tyne, UK. He carries out research which focuses on the challenges associated with the widespread integration and control of distributed/renewable generation in electrical distribution networks. Prior to joining Newcastle University he held the DONG Energy Chair in Renewable Energy and was a Director of the Durham Energy Institute.

Professor Taylor has worked in an advisory capacity to the Department of Energy & Climate Change, Enercon, The Research Council of Norway, The Netherlands Organisation for Scientific Research, and the Ministry of Science, Technology and Innovation in Malaysia relating to Renewable Energy. He is a member of the RCUK Scientific Advisory Committee and non-executive Director of Northern Powergrid. He is a chartered engineer.